Proceedings of ICBioMed 2025 Symposium: AI for Healthcare: Advanced Medical Data Analytics and Smart Rehabilitation
DOI: 10.54254/2753-8818/2025.AU24072

Spatiotemporal Transcriptomic Dissection of Tumor-Associated Macrophage Heterogeneity and Dual-Function Molecular Nodes in Pancreatic Ductal Adenocarcinoma

Mengfei Li

Department of Biology Science, Shandong University, Qingdao, China
202223142018@mail.sdu.edu.cn

Abstract: Many studies have shown that pancreatic cancer is one of the cancers with extremely high mortality. The poor prognosis and lack of early diagnostic methods remain major challenges in the treatment of this cancer. In this article, in order to better detect the occurrence of pancreatic cancer, tools such as monocle3, singleR, harmony in R, and scanpy in Python were used to analyze the cells and genes of pancreatic cancer tissues in mice. By analyzing the data, the following results were obtained: T-cells in healthy PBMCs exhibited broader spatial dispersion than in PDAC tissues, suggesting tumor-driven immune surveillance impairment, while PDAC-associated macrophages displayed expanded distribution linked to pro-tumorigenic functions such as COL1A1-mediated ECM remodeling; Pseudotemporal trajectory analysis revealed myeloid progenitor bifurcation into monocytes/macrophages, with PDAC macrophages showing epigenetically silenced cytotoxic pathways such as suppressed GZMA/NKG7 and enhanced ribosomal biogenesis; Tissue-specific markers such as LCN2 in healthy and CTRB1/AMY2A in PDAC) and spatial co-localization of macrophages/tumor cells highlighted NOP53 as a dual-function hub—inhibiting PI3K-AKT while activating p53—and SPP1 as a paradoxical regulator of metastasis and antitumor immunity; Differential expression and GO enrichment analyses identified ribosomal biogenesis and cytoplasmic translation as PDAC-enriched pathways, contrasting with suppressed stress responses. Our spatial transcriptomic profiling further resolved elevated NOP53, CFB, and SPP1 expression gradients in PDAC tissues, proposing these as diagnostic biomarkers.

Keywords: Pancreatic ductal adenocarcinoma (PDAC), Tumor-associated macrophages (TAMs), Spatial transcriptomics, Single-cell RNA sequencing, Immune suppression, Ribosomal biogenesis

1. Introduction

Pancreatic ductal adenocarcinoma (PDAC), the most prevalent histological subtype of pancreatic cancer[1] represents the seventh leading cause of global cancer-related mortality[2]. The incidence of pancreatic cancer has risen alarmingly worldwide, with projections indicating its persistence as a predominant contributor to oncologic deaths[3]. The absence of pathognomonic clinical manifestations and the lack of robust, minimally invasive diagnostic modalities render early PDAC detection exceptionally challenging[4]. Consequently, most cases are identified at advanced stages,

DOI: 10.54254/2753-8818/2025.AU24072

where current therapeutic interventions exhibit limited efficacy[5], resulting in a dismal prognosis with a five-year survival rate below 10%. Elucidating the molecular pathogenesis of pancreatic cancer remains imperative for developing targeted treatment strategies.

Macrophages, heterogeneous immune cells ubiquitously distributed across all anatomical compartments[6,7], constitute the principal cellular component of leukocytic infiltrates in pathological states[8]. These phagocytic cells demonstrate remarkable phenotypic plasticity, dynamically adapting their functional states in response to microenvironmental stimuli[7,9-11]. Under neoplastic conditions, malignant cells subvert macrophage physiology, driving their transformation into tumor-associated macrophages (TAMs)[12,13]. TAMs facilitate oncogenic progression through paracrine signaling that promotes cellular proliferation, angiogenesis, and metastatic dissemination[13].

The tumor microenvironment (TME), a dynamic network comprising malignant cells, immune populations, stromal fibroblasts, and extracellular matrix constituents[14], exerts bidirectional regulation over macrophage metabolism and polarization. This regulation occurs via direct metabolite exchange or cytokine-mediated signaling[15]. Within the TME, intricate cross-talk between tumor cells, stromal elements, and immune infiltrates drives macrophage differentiation into either protumorigenic or tumor-suppressive phenotypes[14]. TAMs reciprocally modulate the TME by altering cytokine gradients and metabolic landscapes, thereby assuming central roles in antitumor immunity[16]. Substantial clinical evidence implicates macrophages in tumorigenic initiation and malignant progression[6], with TAMs constituting the predominant immune population in the TME and serving as critical mediators of metastatic dissemination[17].

TAMs function as pivotal drivers of therapeutic resistance and metastatic progression[18], sharing functional and phenotypic characteristics with tissue-resident macrophages[19]. As principal immunomodulators within the TME, TAMs directly suppress cytotoxic T lymphocyte and natural killer (NK) cell activation, thereby subverting protective antitumor immunity[20]. Oncogenic transformation of epithelial cells disrupts homeostatic macrophage differentiation pathways, generating parenchymal and stromal TAM subsets that accelerate neoplastic progression[21]. Environmental cues within the TME polarize macrophages toward either proinflammatory M1-like or immunosuppressive M2-like phenotypes[10]. The interaction between macrophage surface receptor SIRPα and tumor cell ligand CD47 generates "don't eat me" signals that inhibit phagocytic clearance[22]. Tumor-derived colony-stimulating factors further reinforce M2 polarization, enhancing TAMs' protumorigenic functions[22].

M2-polarized TAMs predominantly facilitate tumor progression within the TME through secretion of growth-promoting factors[23,24] and orchestration of immunosuppressive mechanisms, including synthesis of inhibitory cytokines (e.g., IL-10, TGF-β), expression of T cell co-inhibitory ligands (e.g., PD-L1), and depletion of essential amino acids required for effector T cell function[25]. Notably, the M2d TAM subtype, activated via TLR ligands and adenosine A2 receptor agonists, critically regulates tumor angiogenesis, metastatic dissemination, and stromal remodeling[26].

PDAC is histologically characterized by a fibroinflammatory stroma enriched with heterogenous immune infiltrates[27,28], cancer-associated fibroblasts (CAFs), extracellular matrix (ECM) proteins, and activated stellate cells[29]. TAMs represent the most abundant immune population within the pancreatic tumor stroma[30], functioning as primary instigators of immunosuppression[31]. From carcinogenic initiation, pancreatic tumors evolve an immunosuppressive TME marked by elevated myeloid-derived suppressor cells (MDSCs), M2-polarized macrophages, and regulatory T cells (Tregs), contrasting with diminished M1 macrophages, dendritic cells, and CD4+/CD8+ effector T lymphocytes[32,33]. Macrophage-derived oncostatin M (OSM) activates CAFs, inducing proinflammatory gene expression that fosters tumor cell survival, migratory capacity, and chemoresistance[34]. M2 macrophages further potentiate angiogenesis via vascular endothelial

DOI: 10.54254/2753-8818/2025.AU24072

growth factor (VEGF) secretion, correlating significantly with increased microvessel density (MVD) in PDAC specimens[35,36].

Single-cell sequencing encompasses genomic or transcriptomic analysis at individual cell resolution, involving cell isolation, nucleic acid amplification, and high-throughput sequencing[37]. In oncologic research, this technology enables clonal evolution analysis, cellular heterogeneity mapping, and functional characterization of rare cell populations[37]. Integration of single-cell RNA sequencing (scRNA-seq) with spatial transcriptomics has advanced understanding of macrophage ontogeny, phenotypic plasticity, and functional adaptation within tumors[38]. Pseudotemporal trajectory analysis reconstructs cellular differentiation dynamics, revealing transitional states during macrophage evolution[39].

Spatial transcriptomics employs single-molecule fluorescence in situ hybridization (smFISH) to localize mRNA transcripts within tissue sections[40]. Released mRNAs bind spatially barcoded oligonucleotide arrays, enabling reverse transcription into complementary DNA (cDNA) with positional fidelity. Subsequent sequencing and computational alignment generate high-resolution maps of gene expression topography[40]. In cancer studies, this methodology elucidates tumor heterogeneity, delineates cellular interaction networks within the TME, and uncovers molecular mechanisms underlying neoplastic initiation and progression[41]. For instance, spatial transcriptomics has resolved the spatial distribution and functional states of tumor-infiltrating macrophages while quantifying gene expression gradients across discrete tissue regions[40,41].

In summary, the complex interplay between TAM-driven immunosuppression, stromal remodeling, and metabolic adaptation underscores PDAC's therapeutic intractability. While single-cell and spatial transcriptomic technologies have provided unprecedented insights into macrophage heterogeneity and TME dynamics, critical gaps remain in understanding how spatiotemporal coordination of these processes dictates PDAC progression and therapeutic resistance. Our study integrates multi-omics approaches to dissect the functional crosstalk between transcriptional reprogramming and spatial architecture in PDAC, aiming to identify novel therapeutic vulnerabilities by bridging molecular mechanisms with their spatial context.

2. Methods

Data Acquisition:

The single-cell data from human samples were sourced from GEO[42]。The dataset was derived from high-throughput sequencing-based expression profiling analysis. The repository encompasses 16 PDAC tissue specimens, 3 adjacent normal pancreatic tissue samples, 16 PBMC samples obtained from human PDAC patients, and 4 PBMC samples from healthy volunteers. The tissues were subjected to mechanical mincing and enzymatic digestion using collagenase P (1 mg/mL DMEM), followed by filtration through a 40 μm mesh to isolate single cells. Subsequently, dead cells were eliminated utilizing the MACS® Dead Cell Removal Kit (Miltenyi Biotec Inc.). Single-cell cDNA libraries were constructed and sequenced on the 10x Genomics platform at the University of Michigan Sequencing Core. The sequencing was performed on HiSeq 4000 or NovaSeq 6000 (Illumina) instruments, employing paired-end 50-cycle reads with a sequencing depth of 100,000 reads per sample. The raw sequencing data were processed and aligned by the University of Michigan DNA Sequencing Core. Cellranger count version 3.0.0 was employed with default parameters, with an initial anticipated cell count set at 10,000.

The spatial transcriptomic dataset for human pancreatic cancer samples was obtained from the 10x Genomics repository [43]. Formalin-Fixed Paraffin-Embedded (FFPE) tissue blocks, characterized by adenocarcinoma of grade I-II with approximately 50% tumor content, were sourced from AcePix Biosciences. Tissue preparation was conducted in accordance with the demonstrated protocols

DOI: 10.54254/2753-8818/2025.AU24072

outlined in the Xenium In Situ Tissue Preparation Guide for FFPE (CG000578) and Xenium In Situ Dewaxing and Decrosslinking for FFPE Tissue (CG000580). The gene panel utilized was the Xenium Human Multi-Tissue and Cancer Panel, which was pre-designed by 10x Genomics and informed by single-cell RNA sequencing data that were curated and standardized by the Human Protein Atlas. The panel comprises 93 genes specifically selected to detect major cell types in breast, lung, kidney, liver, skin, colon, heart, lymph node, and pancreas tissues, as well as 284 genes designed to be common across all tissues, with an emphasis on immune and cancer markers. This pre-designed panel was further supplemented with an additional 97 genes, including high expressers, to evaluate potential sensitivity loss due to gene crowding. The Xenium Analyzer was operated following the Xenium Analyzer User Guide (CG000584), and the on-instrument analysis was conducted using Xenium Onboard Analysis version 1.6.0.

Filtering and normalization of scRNA-seq data:

In this experiment, Seurat v5 was utilized. Cells with less than or more than 200 expressed genes and genes expressed in fewer than 3 cells were filtered out. Cells with mitochondrial gene expression exceeding 5% were also filtered out.The remaining cells and gene subsets were used for subsequent analysis.

Dimensional reduction and clustering:

Integrated analysis was conducted using Harmony for four healthy PBMC(Peripheral Blood Mononuclear Cells) samples, four PBMC samples from patients with PDAC(pancreatic ductal adenocarcinoma), four PDAC tissue samples, and three adjacent normal tissue samples. Additionally, cell annotation was performed for each sample using SingleR. During the clustering process with Harmony integration, the top 30 dimensions were selected. The dimensionality reduction method used was Principal Component Analysis (PCA).

Pseudotime analysis:

The subsets of cell types including macrophages, monocytes, and CMPs were extracted from each of the integrated files using the subset method, resulting in integrated data for these three cell types across the four integrated datasets. Then, CMP was selected as the root cells, and Monocle3 was used to learn the cellular trajectory. After learning the cellular trajectory, the top 10 genes expressed in macrophages were selected for differential gene expression analysis.

Gene Expression Differential Analysis:

The logFC values for each gene in a total of 41 samples were obtained using FindAllMarkers, with the parameter threshold set to 0.25. The samples were divided into two groups: adjacent normal tissues versus PDAC, and healthy PBMC versus PDAC PBMC, for differential gene expression analysis.

Gene Enrichment Analysis:

Gene enrichment analysis was conducted on the data obtained from the differential gene expression analysis using both GO and KEGG excluding data with a p-value less than 0.05, respectively.

Spatial transcriptome

Spatial transcriptomic analysis was performed using Squidpy (Spatial Quantitative Imaging of Differential gene expression in Python). The spatial distributions of ductal cells, macrophages, and tumor cells were mapped, and the spatial patterns of gene expression abundance within macrophages were visualized.

3. Result

To elucidate cell type-specific clustering patterns across four distinct sample categories, we implemented Harmony for batch effect correction and dataset integration. Principal Component Analysis (PCA) was applied for dimensionality reduction, followed by UMAP visualization to

DOI: 10.54254/2753-8818/2025.AU24072

resolve intrinsic clustering architectures. This pipeline effectively preserved biological heterogeneity while mitigating technical variability across samples. Comparative analysis revealed that T-cells in healthy peripheral blood mononuclear cells (PBMCs) exhibited broader spatial dispersion relative to pancreatic ductal adenocarcinoma (PDAC) tissues (Figures 1c, 1f). Conversely, macrophages in PDAC tissues displayed expanded distribution compared to adjacent non-tumor regions (Figures 2c, 2f).

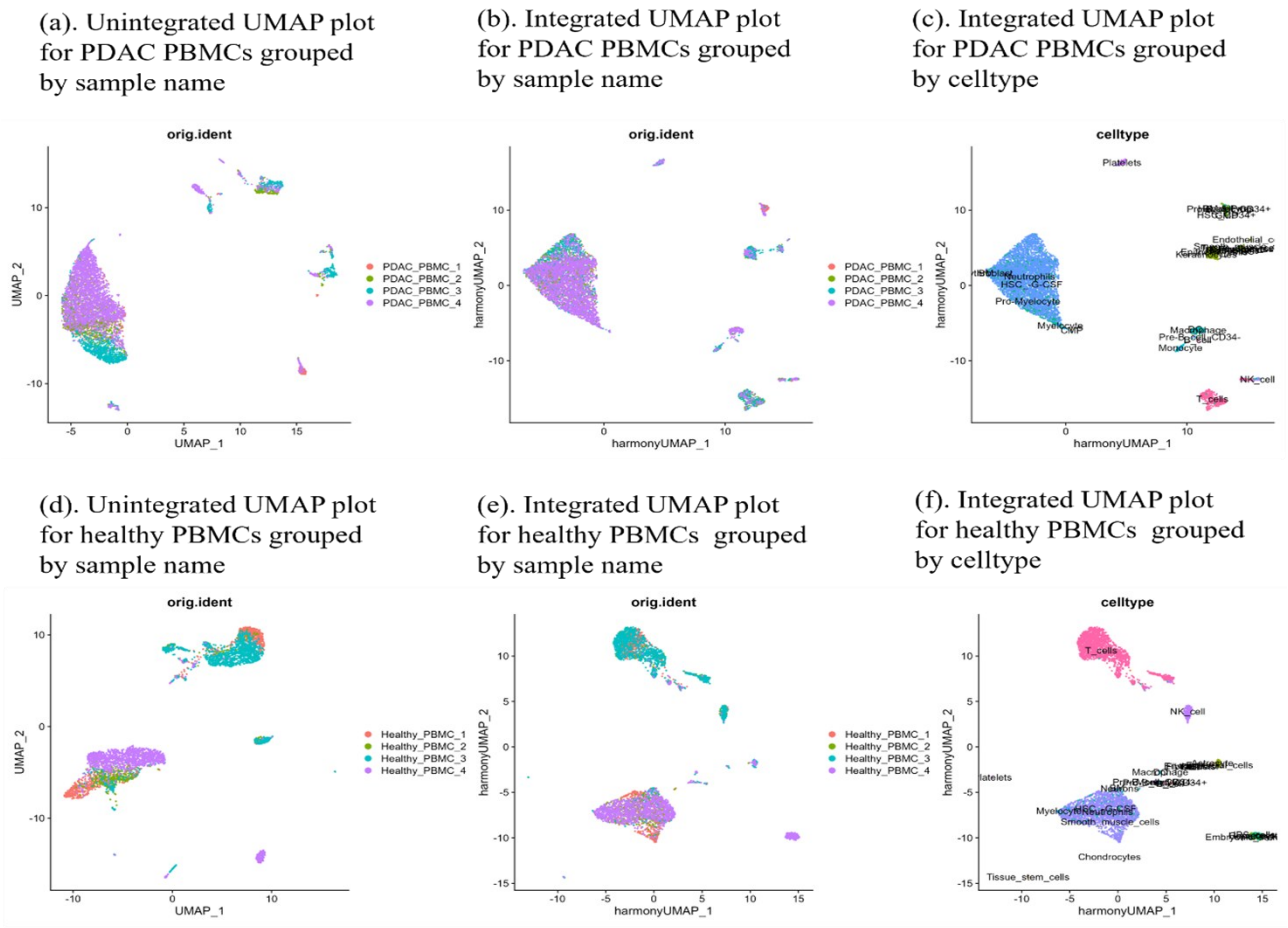

Panels (a)-(c) show unintegrated and harmony-integrated UMAP plots for the first four samples of PDAC PBMCs. Panel (a) displays the unintegrated UMAP plot categorized by sample name, panel (b) shows the harmony-integrated UMAP plot categorized by sample name, and panel (c) presents the harmony-integrated UMAP plot categorized by cell type.Panels (d)-(f) show unintegrated and harmony-integrated UMAP plots for the first four samples of healthy PBMCs. Panel (d) displays the unintegrated UMAP plot categorized by sample name, panel (e) shows the harmony-integrated UMAP plot categorized by sample name, and panel (f) presents the harmony-integrated UMAP plot categorized by cell type.

Figure 1: UMAP plots and harmony - integrated for PDAC tissue and adjacent normal tissue

DOI: 10.54254/2753-8818/2025.AU24072

(a). Unintegrated UMAP plot for PDAC tissue grouped by sample name

(b). Integrated UMAP plot for PDAC tissue grouped by sample name

(c). Integrated UMAP plot for PDAC tissue grouped by celltype

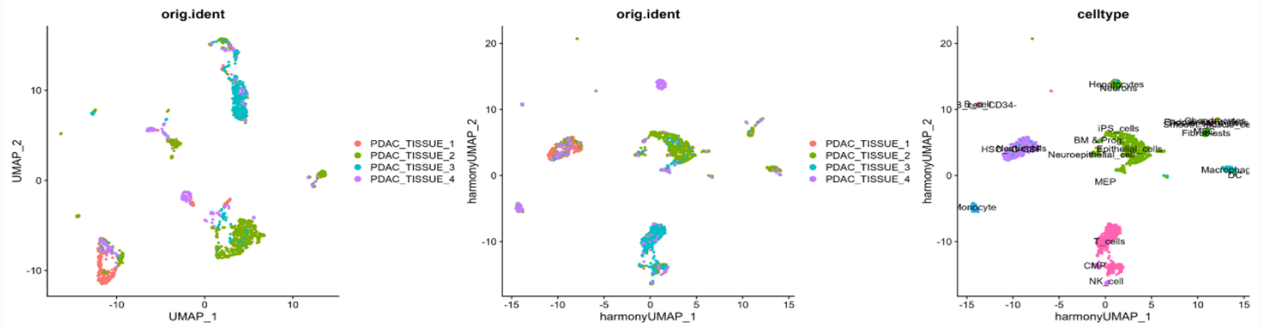

(d). Unintegrated UMAP plot for adjacent normal tissue grouped by sample name

(e). Integrated UMAP plot for adjacent normal tissue grouped by sample name

(f). Integrated UMAP plot for adjacent normal tissue grouped by celltype

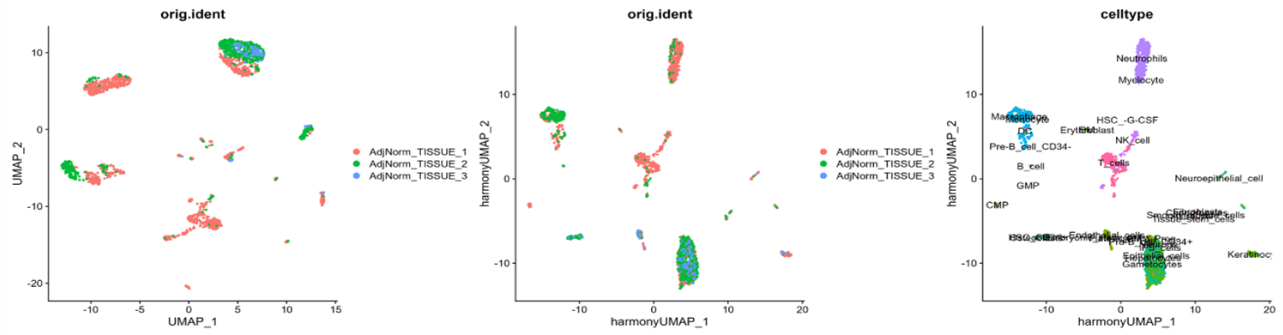

Panels (a)-(c) show unintegrated and harmony-integrated UMAP plots for the first four samples of pancreatic ductal adenocarcinoma (PDAC) tissue. Panel (a) displays the unintegrated UMAP plot categorized by sample name, panel (b) shows the harmony-integrated UMAP plot categorized by sample name, and panel (c) presents the harmony-integrated UMAP plot categorized by cell type. Panels (d)-(f) show unintegrated and harmony-integrated UMAP plots for the first four samples of adjacent normal tissue. Panel (d) displays the unintegrated UMAP plot categorized by sample name, panel (e) shows the harmony-integrated UMAP plot categorized by sample name, and panel (f) presents the harmony-integrated UMAP plot categorized by cell type.

Figure 2: UMAP plots and harmony - integrated for PDAC tissue and adjacent normal tissue

To profile transcriptional heterogeneity across cell types, we generated bubble plots with cell types annotated on the x-axis and gene symbols on the y-axis. Bubble size quantifies expression magnitude, while color gradients denote detection frequency, enabling simultaneous visualization of quantitative and qualitative expression features. Notably, the top 10 highly expressed genes in healthy PBMCs demonstrated marked divergence from PDAC PBMCs (Figures 3a, 3b). Tissue-specific markers were identified: LCN2 dominated in healthy tissues, whereas CTRB1 was upregulated in PDAC. Adjacent normal tissues showed preferential expression of SDPR, while AMY2A was enriched in PDAC regions (Figures 4a, 4b).

DOI: 10.54254/2753-8818/2025.AU24072

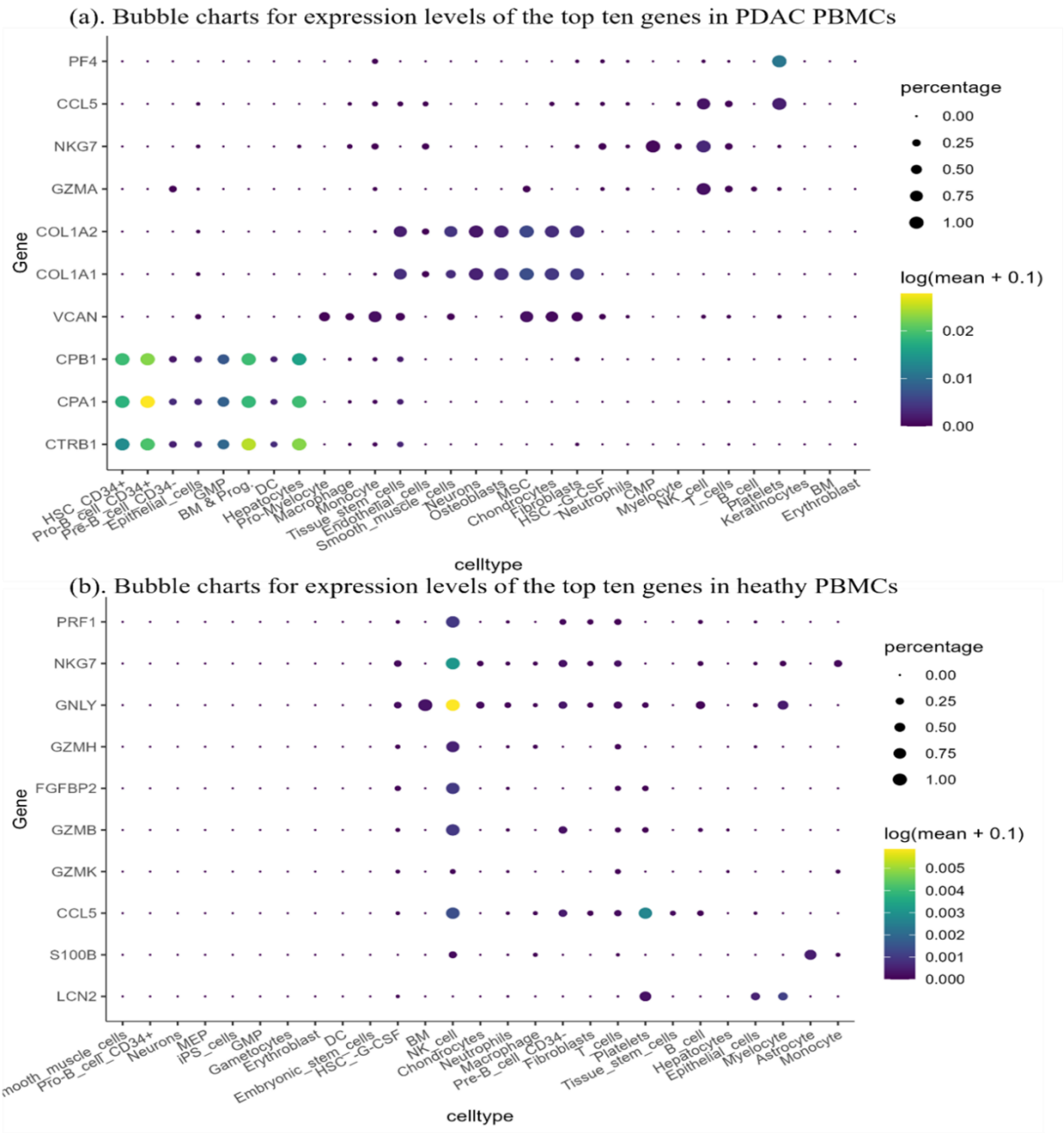

Figure a displays the expression levels of the top ten genes with the highest expression in each cell within the integrated PDAC PBMC samples. Figure b shows the expression levels of the top ten genes with the highest expression in each cell within the integrated healthy PBMC samples.

Figure 3: Bubble charts for expression levels of the top ten genes in PDAC PBMCs and healthy PBMCs

DOI: 10.54254/2753-8818/2025.AU24072

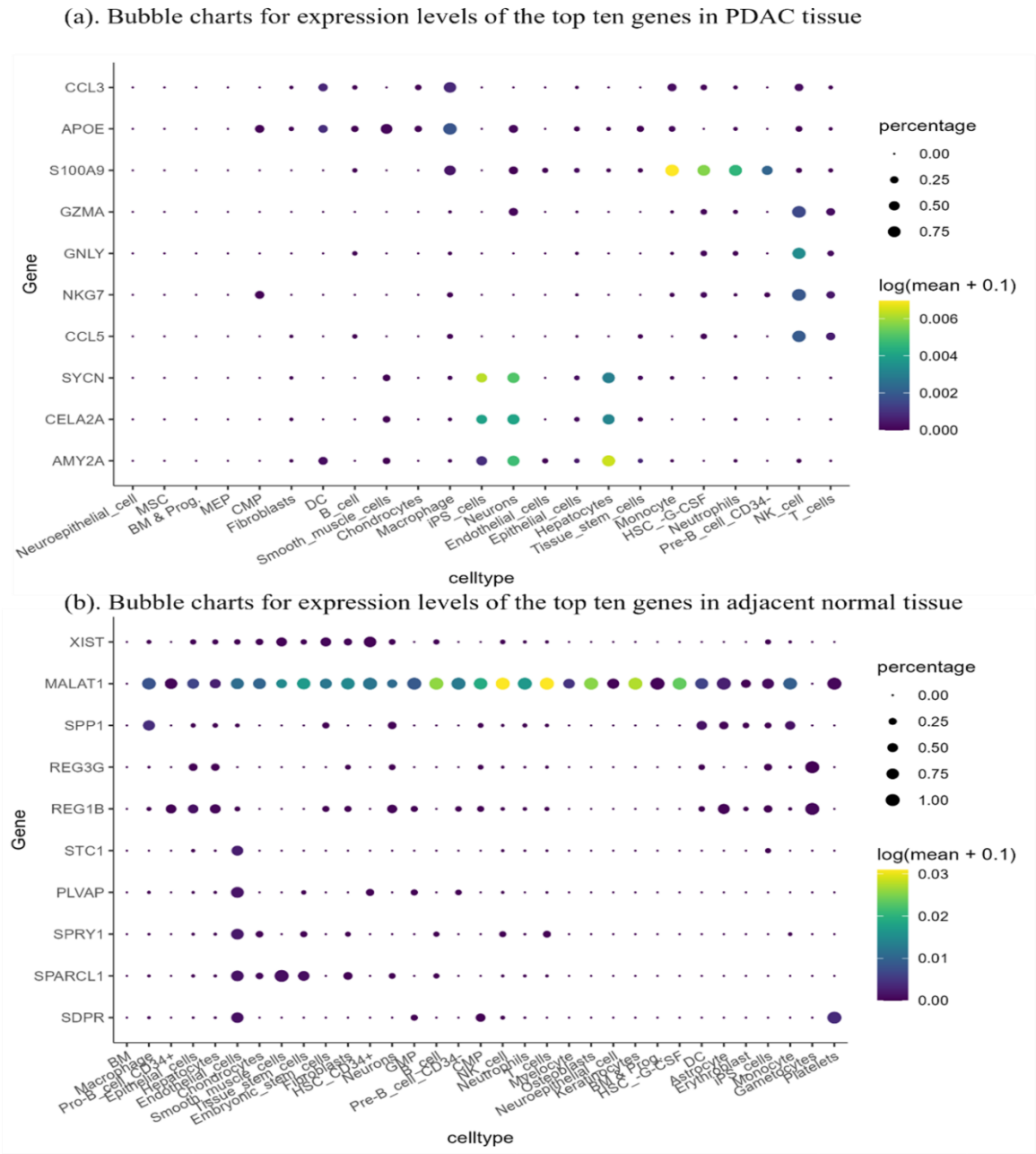

Figure a displays the expression levels of the top ten genes with the highest expression in each cell within the integrated PDAC tissue samples. Figure b shows the expression levels of the top ten genes with the highest expression in each cell within the integrated adjacent normal tissue samples.

Figure 4: Expression levels of the top ten genes in PDAC tissue and adjacent normal tissue

Pseudotime analysis using single-cell RNA sequencing (scRNA-seq) data reconstructed macrophage differentiation dynamics. By ordering cells along a pseudotemporal continuum based on transcriptional similarity, we delineated transitional states and lineage commitment patterns. Integrated trajectory analysis revealed that common myeloid progenitors (CMPs) bifurcated into monocytes and macrophages during development (Figure 5,6).

DOI: 10.54254/2753-8818/2025.AU24072

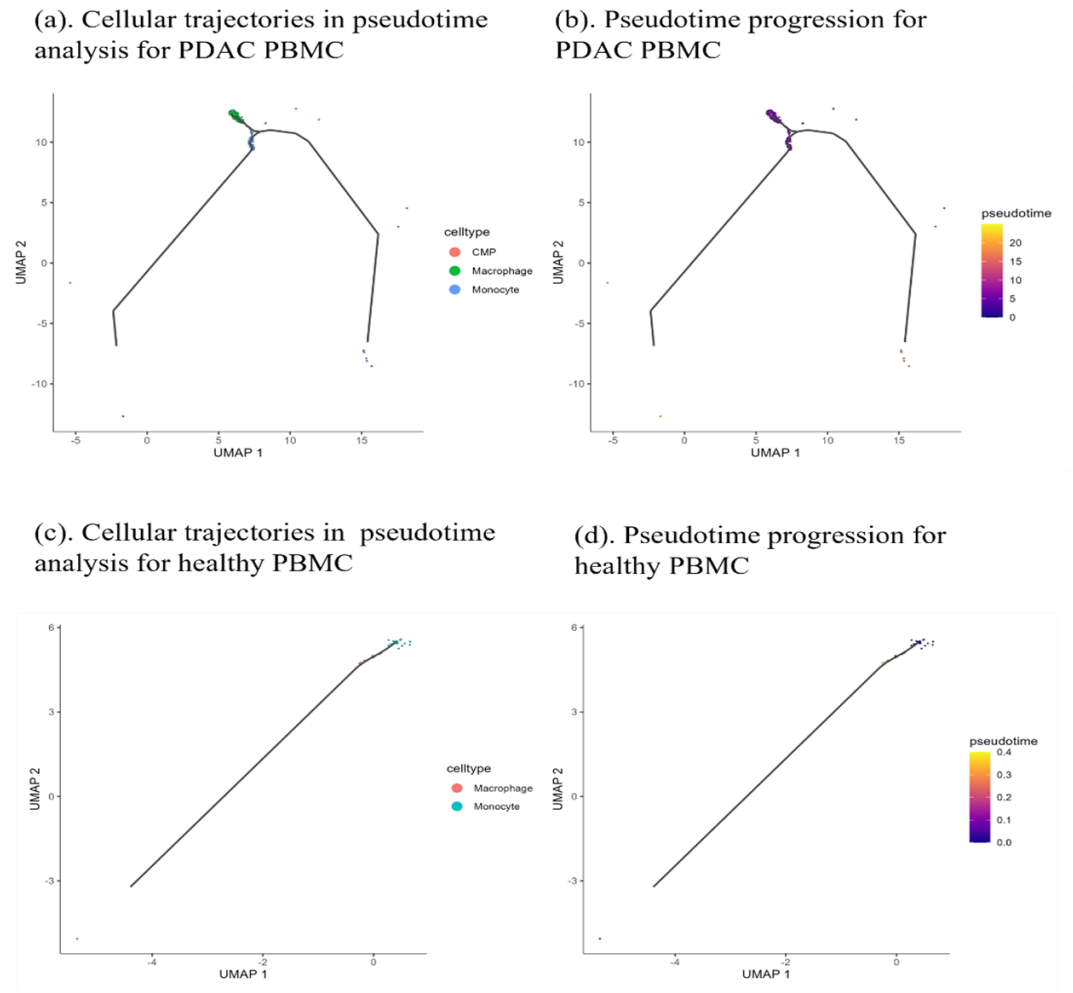

Figures a, c present the cellular trajectories in pseudotime analysis for PDAC PBMC and healthy PBMC , respectively, with cell types distinguished by different colors. Alternatively, figures b, d focus on the pseudotime progression within these same samples, where different colors now represent different stages of pseudotime.

Figure 5: Pseudotime analysis for macrophage in PDAC PBMC, healthy PBMC, PDAC tissue, and adjacent normal tissue

DOI: 10.54254/2753-8818/2025.AU24072

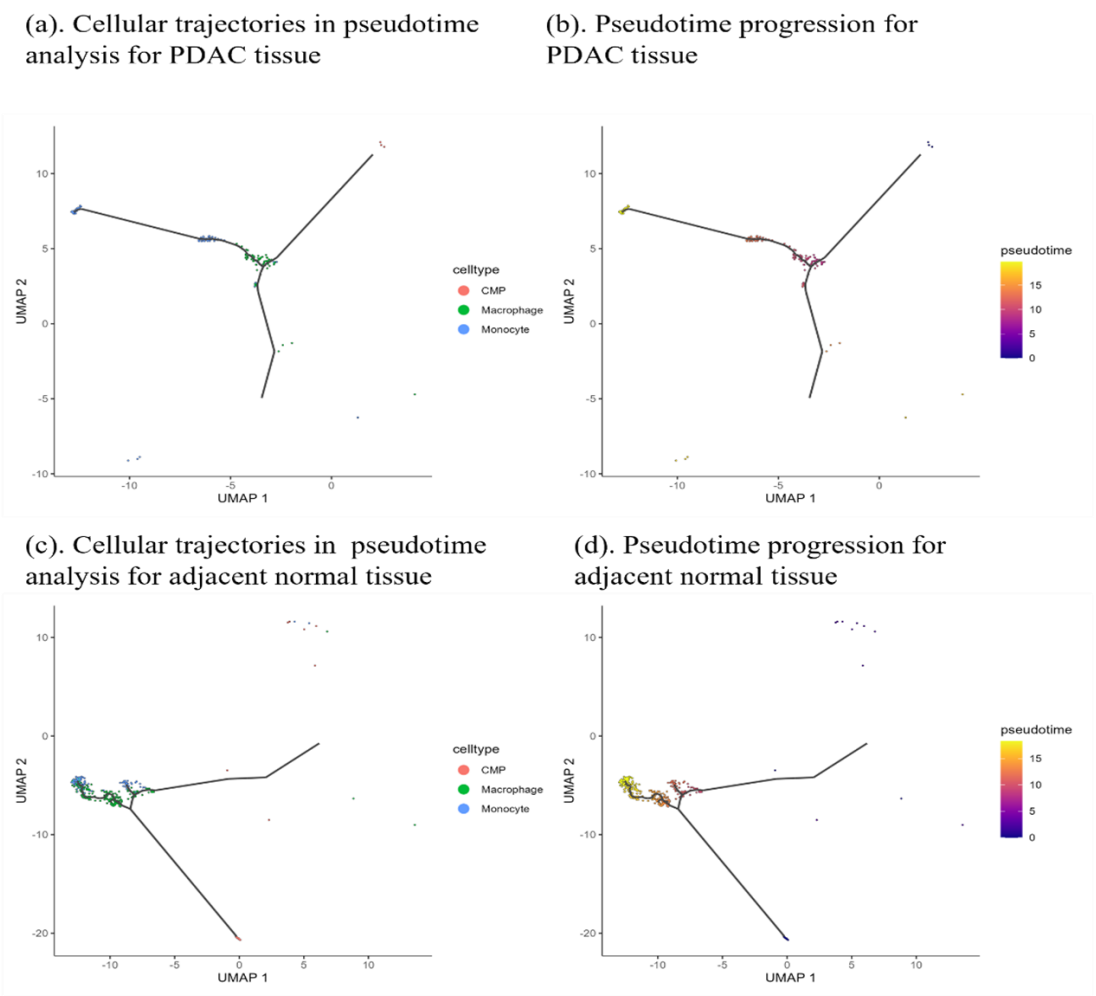

Figures a, c present the cellular trajectories in pseudotime analysis for PDAC tissue and adjacent normal tissue, respectively, with cell types distinguished by different colors. Alternatively, figures b, d focus on the pseudotime progression within these same samples, where different colors now represent different stages of pseudotime.

Figure 6: Pseudotime analysis for macrophage in PDAC PBMC, healthy PBMC, PDAC tissue, and adjacent normal tissue

UMAP visualization mapped spatial heterogeneity in macrophage gene expression across sample types. Transcript abundance was encoded by a continuous color gradient, with darker hues indicating elevated expression. In PDAC-associated macrophages, GZMA, COL1A1, and PF4 exhibited broad expression, while NKG7, VCAN, CCL5, CPA1, CPB1, and CTRB1 showed restricted ranges (Figure 7a). Healthy macrophages predominantly expressed GZMK, LCN2, GZMB, FGFBP2, and PRF1 (Figure 7a). PDAC tissues were enriched for S100A9, APOE, and CCL3, whereas adjacent normal regions overexpressed STC1, MALAT1, and SPP1 (Figures 8a, 8b).

DOI: 10.54254/2753-8818/2025.AU24072

(a). UMAP plot for the top ten genes with the highest expression in macrophages within PDAC PBMC

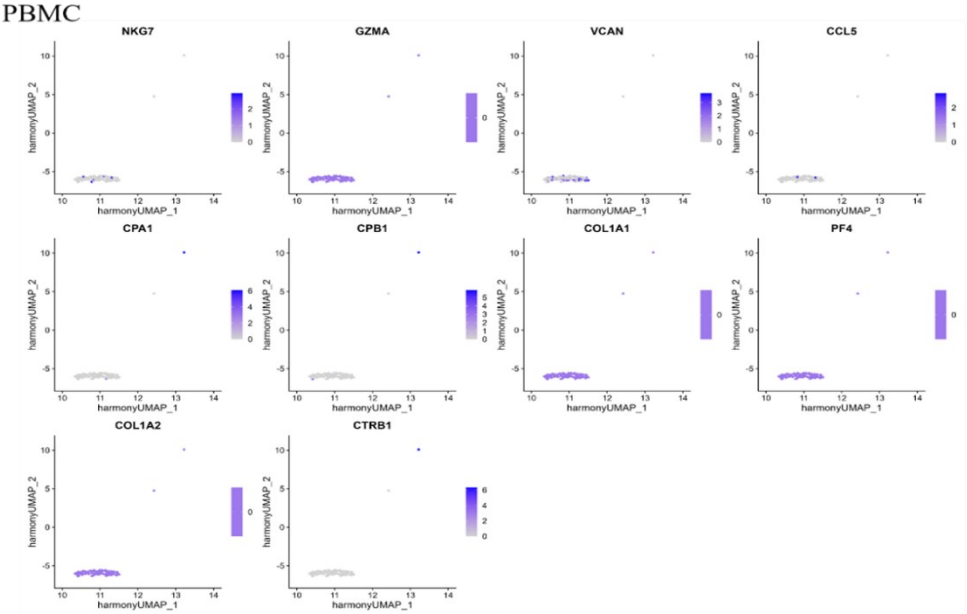

(b). UMAP plot for the top ten genes with the highest expression in macrophages within PDAC PBMC

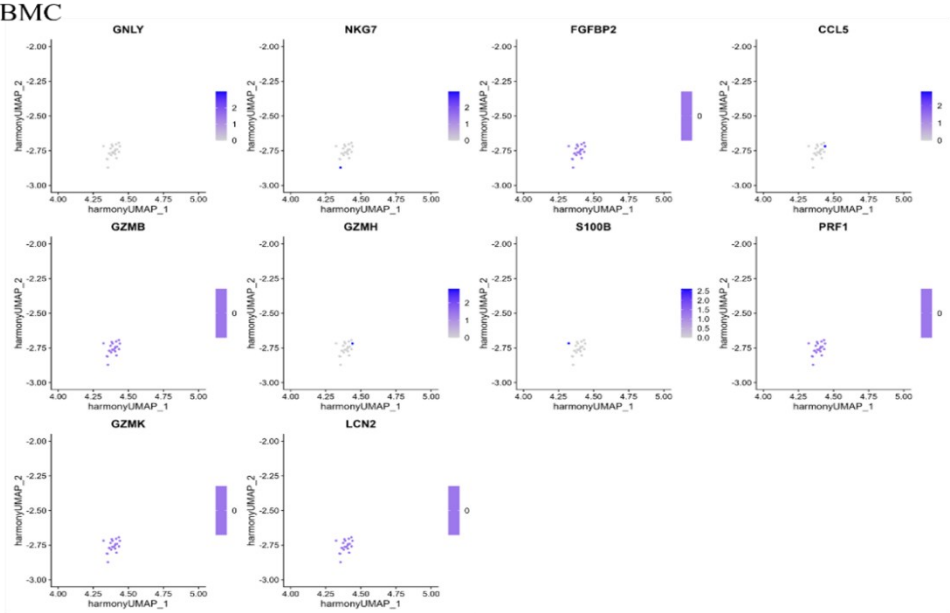

Figure a displays the UMAP plot for the top ten genes with the highest expression in macrophages within the integrated PDAC PBMC samples. Figure b shows the UMAP plot for the top ten genes with the highest expression in macrophages within the integrated healthy PBMC samples.

Figure 7: UMAP plot for the top ten genes with the highest expression in macrophages within the PDAC PBMC and healthy PBMC

DOI: 10.54254/2753-8818/2025.AU24072

(a). UMAP plot for the top ten genes with the highest expression in macrophages within PDAC tissue

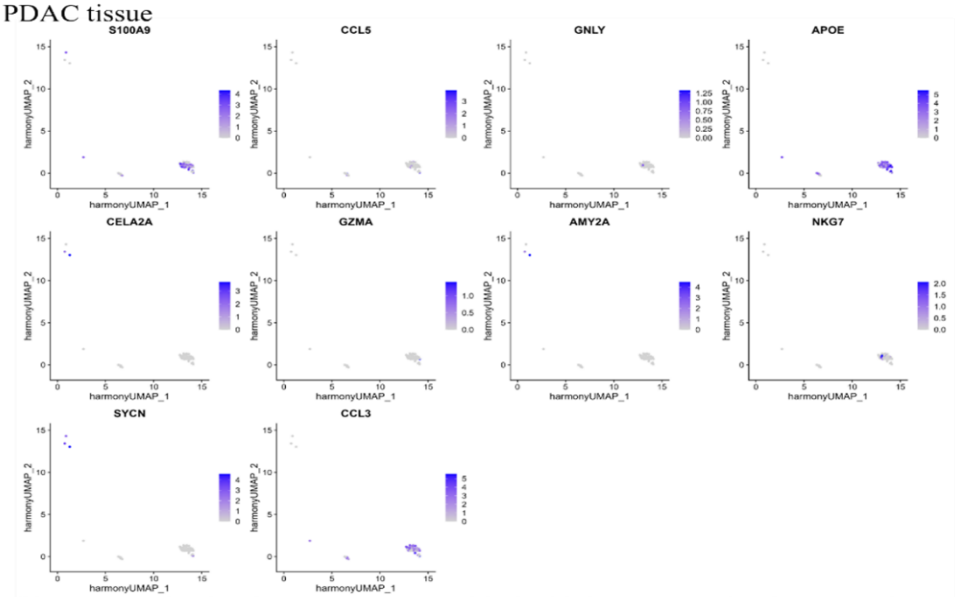

(b). UMAP plot for the top ten genes with the highest expression in macrophages within adjacent normal tissue

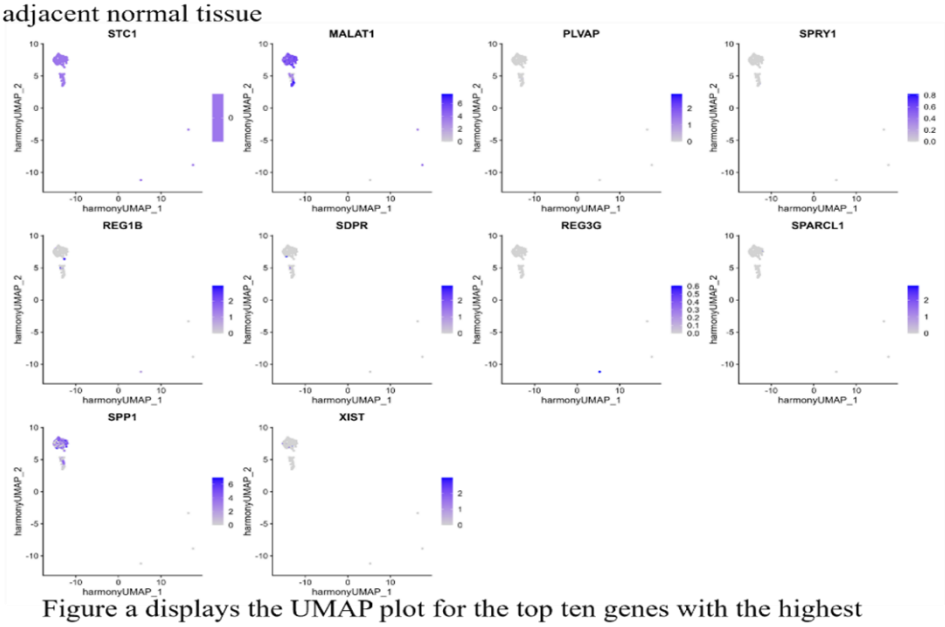

Figure a displays the UMAP plot for the top ten genes with the highest expression in macrophages within the integrated PDAC tissue samples. Figure b shows the UMAP plot for the top ten genes with the highest expression in macrophages within the integrated adjacent normal tissue samples.

Figure 8: UMAP plot for the top ten genes with the highest expression in macrophages within the PDAC tissue and adjacent normal tissue

To elucidate the temporal expression patterns of genes in macrophages along pseudotime, pseudotime trajectory analysis was performed using monocle3. The expression levels of genes exhibited relatively stable trends across pseudotime in macrophages from the following four groups: healthy PBMCs, PDAC PBMCs, PDAC tissue, and adjacent normal tissue(Figure 9,10).

DOI: 10.54254/2753-8818/2025.AU24072

(a). Gene expression difference plot based on pseudotime analysis for the top ten genes with the highest expression in macrophages within the PDAC PBMC

(b). Gene expression difference plot based on pseudotime analysis for the top ten genes with the highest expression in macrophages within the healthy PBMC

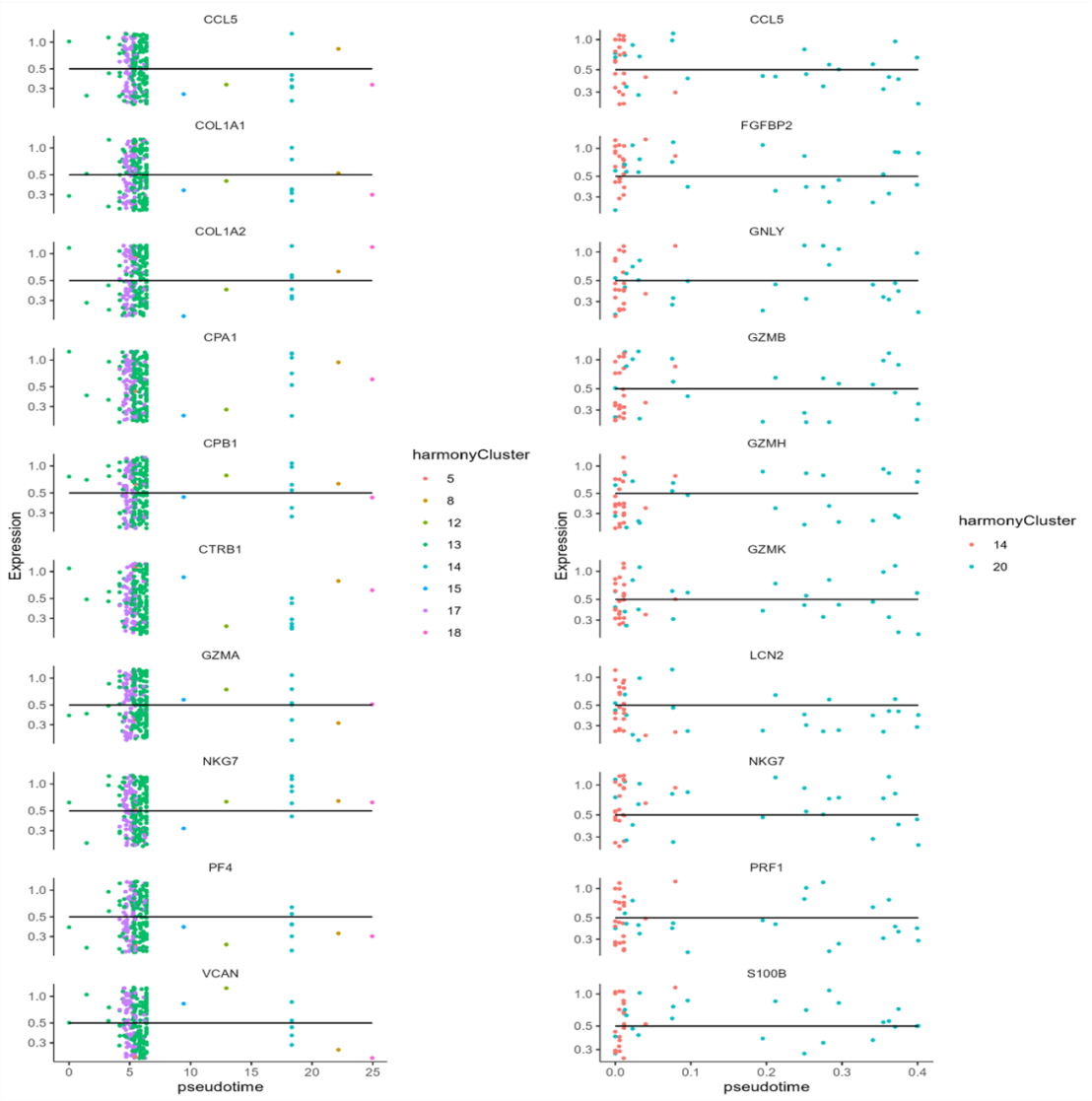

Figure a presents a gene expression difference plot based on pseudotime analysis for the top ten genes with the highest expression in macrophages within the integrated PDAC PBMC samples. Figure b shows a similar gene expression difference plot for the top ten genes in macrophages within the integrated healthy PBMC samples, also based on pseudotime analysis.

Figure 9: Gene expression difference plot based on pseudotime analysis for the top ten genes with the highest expression in macrophages

DOI: 10.54254/2753-8818/2025.AU24072

(a). Gene expression difference plot based on pseudotime analysis for the top ten genes with the highest expression in macrophages within the PDAC tissue

(b). Gene expression difference plot based on pseudotime analysis for the top ten genes with the highest expression in macrophages within the adjacent normal tissue

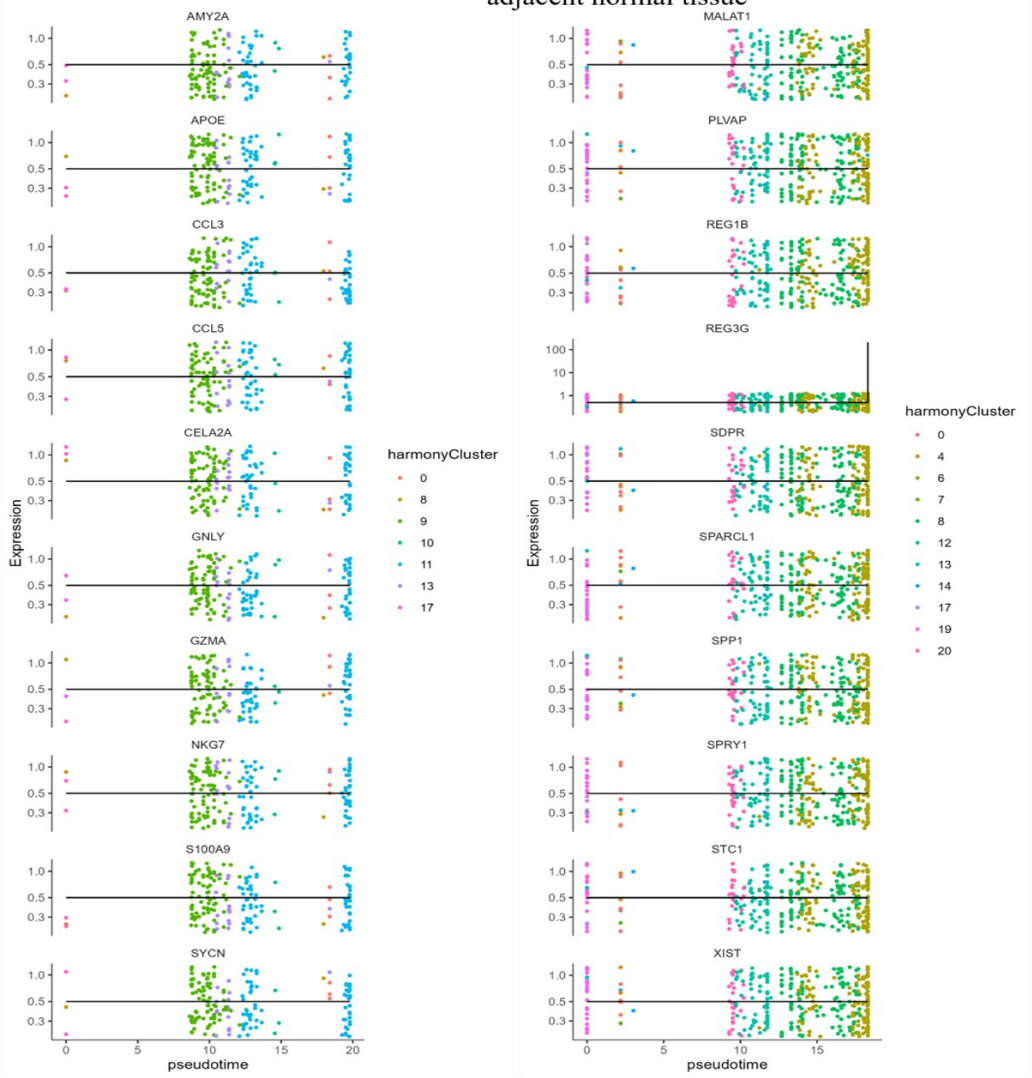

Figure a presents a gene expression difference plot based on pseudotime analysis for the top ten genes with the highest expression in macrophages within the integrated PDAC tissue samples. Figure b shows a similar gene expression difference plot for the top ten genes in macrophages within the integrated adjacent normal tissue samples, also based on pseudotime analysis.

Figure 10: Gene expression difference plot based on pseudotime analysis for the top ten genes with the highest expression in macrophages

DESeq2-based differential expression analysis identified three genes significantly upregulated in PDAC PBMCs versus healthy controls (Figure 11a). In PDAC tissues, 18 genes were upregulated alongside broad downregulation of multiple loci (Figure 11b).Gene Ontology (GO) enrichment revealed distinct pathway activation:Tissues: Ribosomal biogenesis (small subunit), rRNA processing, cytoplasmic translation, and amino acid metabolism were robustly activated. Conversely, pathways regulating multicellular processes, signal transduction, and stress responses were suppressed (Figures 12b, 13b).PBMCs: Cytoplasmic translation and protein metabolism dominated activated pathways, while macromolecule biosynthesis showed partial suppression (Figures 12a, 13a).

DOI: 10.54254/2753-8818/2025.AU24072

(a). Heatmap generated using DEseq2 results for all PBMC samples

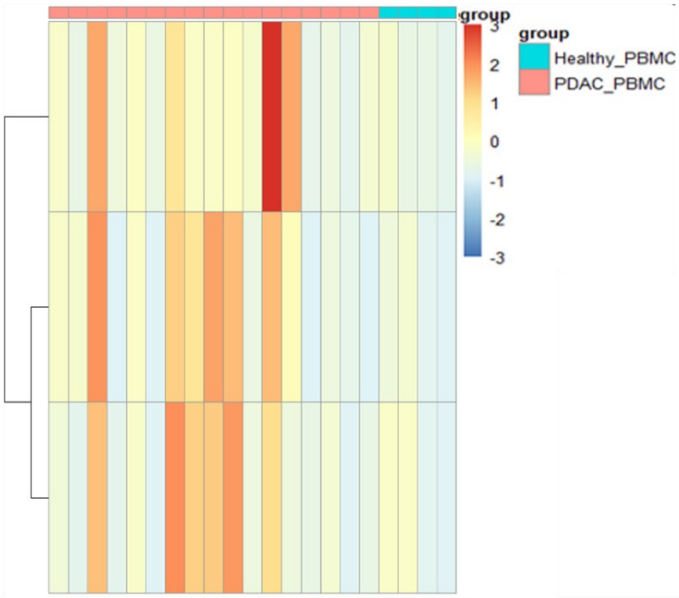

(b). Heatmap created using DEseq2 results for all tissue samples

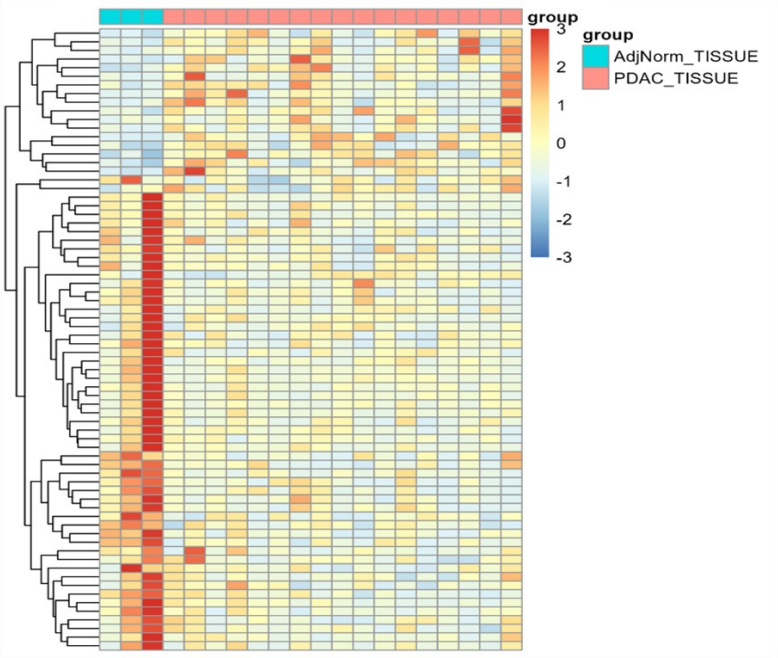

Figure a is a heatmap generated using DEseq2 results for all PBMC samples. In the horizontal columns, blue represents different healthy PBMC samples, and red represents different PDAC PBMC samples. The vertical columns represent different genes. Figure b is a heatmap created using DEseq2 results for all tissue samples. In the horizontal columns of this heatmap, blue represents different adjacent normal tissue samples, and red represents different PDAC tissue samples. The vertical columns, as in Figure a, represent different genes.

Figure 11: Heatmap for all PBMCs and tissue samples

DOI: 10.54254/2753-8818/2025.AU24072

(a). Enrichplot obtained from GO gene enrichment analysis of the data processed using DEseq2 for all PBMC samples

(b). Enrichplot obtained from GO gene enrichment analysis of the data processed using DEseq2 for all tissue samples

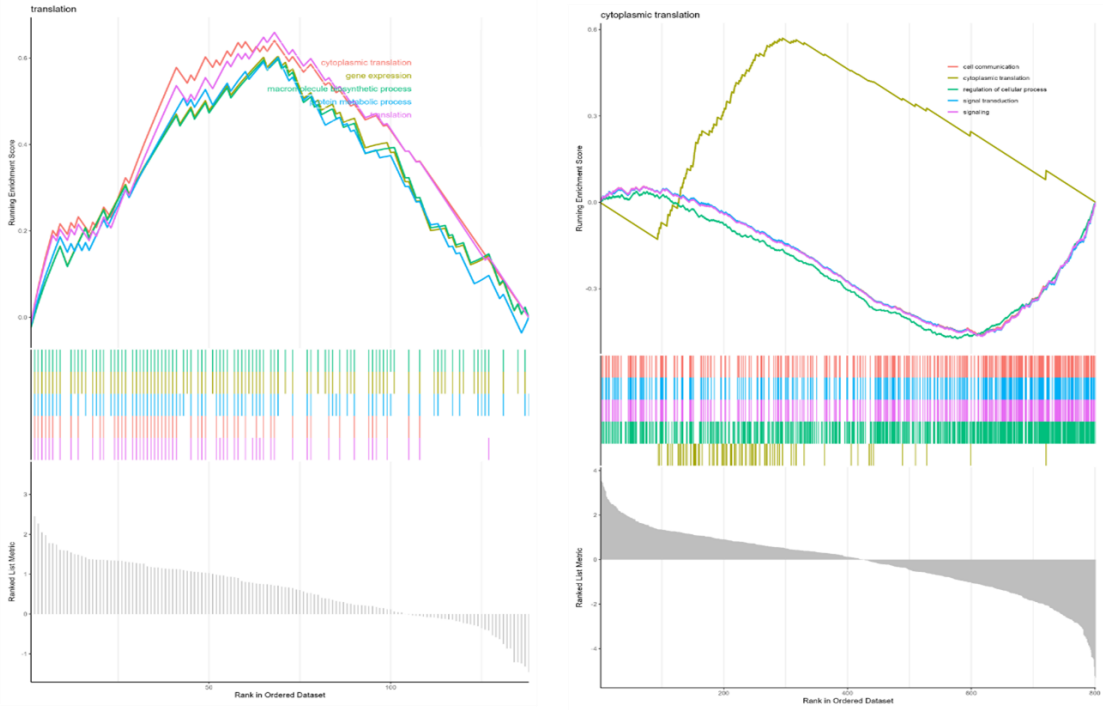

Figure a present the enrichplot obtained from GO gene enrichment analysis of the data processed using DEseq2 for all PBMC samples. Figure show the corresponding enrichplot for the data processed using DEseq2 for all tissue samples and analyzed with GO gene enrichment.

Figure 12: Enrichplot

Spatial transcriptomic profiling resolved the topographic relationship between macrophages and tumor cells, demonstrating uniform tissue distribution (Figure 13a). High-resolution analysis identified NOP53 as the most abundantly expressed gene, followed by CFB, PPA1, CFTR, GATM, SERPINB1, and ANPEP (Figures 13b, 14a).Key Innovations:Multi-Omics Integration: Harmonized single-cell and spatial transcriptomics to dissect cell type-specific dynamics.Trajectory Inference: Uncovered myeloid lineage commitment via pseudotemporal ordering.Pathway Prioritization: Identified ribosomal biogenesis and stress response as central regulatory nodes in PDAC.This systematic framework advances precision oncology by decoding transcriptional circuits driving PDAC progression and microenvironment remodeling.

DOI: 10.54254/2753-8818/2025.AU24072

(a). Dotplot, and ridgeplot obtained from GO gene enrichment analysis of the data processed using DEseq2 for all PBMC samples

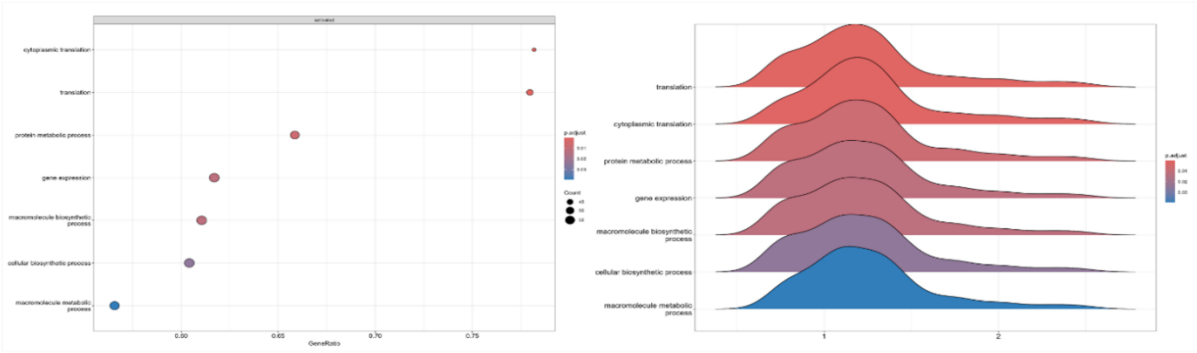

(b). dotplot, and ridgeplot obtained from GO gene enrichment analysis of the data processed using DEseq2 for all tissue samples

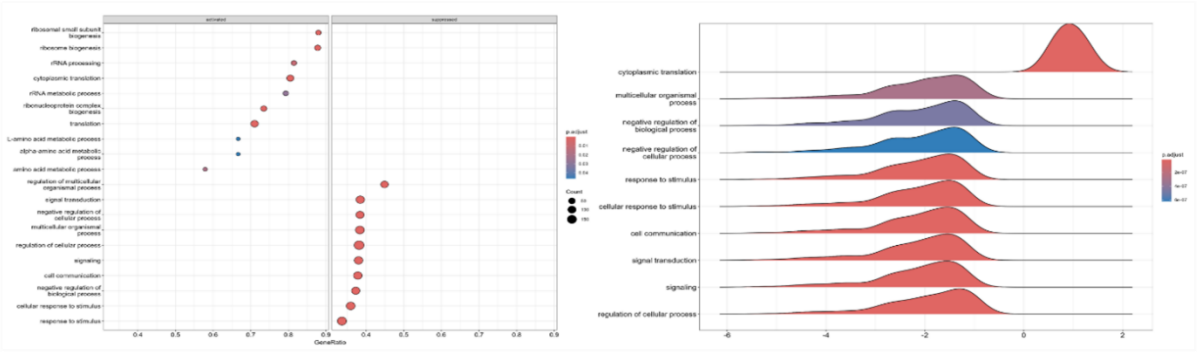

Figure a present the dotplot, and ridgeplot obtained from GO gene enrichment analysis of the data processed using DEseq2 for all PBMC samples. Figure b present the dotplot, and ridgeplot obtained from GO gene enrichment analysis of the data processed using DEseq2 for all tissue samples.

Figure 13: Dotplot, and ridgeplot obtained from GO gene enrichment analysis of the data processed using DEseq2

DOI: 10.54254/2753-8818/2025.AU24072

(a). Distribution map of cells

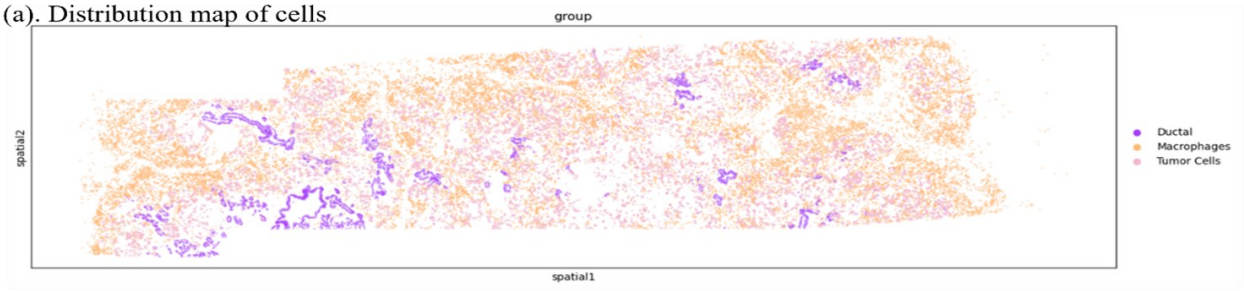

(b). Distribution map of the expression of different genes in macrophages

Figure a is a spatial distribution map of cells obtained from spatial transcriptomics analysis of PDAC tissue sample, with different colors representing different cell types. Figure b is a spatial distribution map of the expression of different genes in macrophages within the samples, where a yellower color indicates higher expression levels.

Figure 14: Spatial transcriptome results

DOI: 10.54254/2753-8818/2025.AU24072

(a). Distribution map of the expression of different genes in macrophages

Figure a is a spatial distribution map of the expression of different genes in macrophages within the samples, where a yellower color indicates higher expression levels.

Figure 15: Distribution map of the expression of different genes

DOI: 10.54254/2753-8818/2025.AU24072

(a). Distribution map of the expression of different genes in macrophages

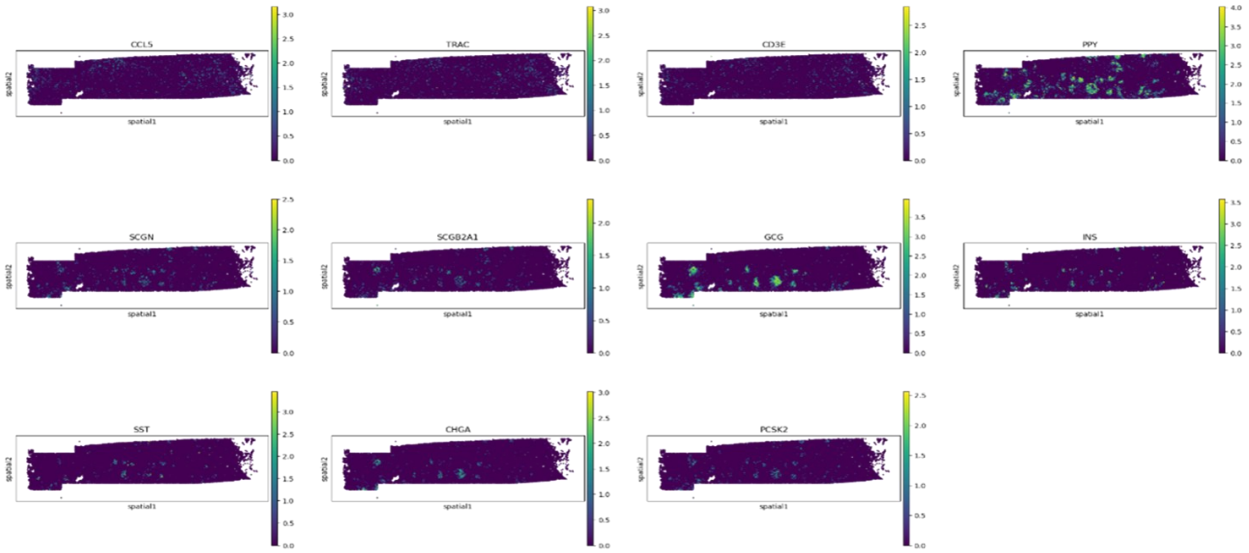

Figure a is a spatial distribution map of the expression of different genes in macrophages within the samples, where a yellower color indicates higher expression levels.

Figure 16: Distribution map of the expression of different genes

4. Discussion

In this study, the integrated multi-omics approach delineates the interplay between transcriptional reprogramming and spatial organization in PDAC pathogenesis. The observed broader spatial dispersion of T-cells in healthy PBMCs compared to PDAC tissues may reflect immune surveillance attenuation in tumor microenvironments, where cytotoxic T-cell infiltration is constrained. Conversely, the expanded distribution of macrophages in PDAC tissues aligns with their tumor-educated phenotypic plasticity, facilitating pro-tumorigenic functions such as extracellular matrix remodeling such as COL1A1 expression and immunosuppression.

The transcriptional divergence between healthy and PDAC PBMCs, particularly in the top 10 highly expressed genes, underscores systemic immune modulation even in circulating cells. Tissue-specific markers like LCN2 (healthy) and CTRB1 (PDAC) not only serve as diagnostic signatures but also highlight metabolic rewiring in PDAC, where CTRB1—a chymotrypsin isoform—may promote nutrient acquisition in nutrient-scarce tumor niches.

Pseudotime trajectory analysis revealed that myeloid progenitors bifurcate into monocytes and macrophages, with PDAC-associated macrophages exhibiting stable yet functionally distinct gene expression patterns. The restricted expression of cytotoxic mediators in PDAC macrophages, contrasted with their robust expression in healthy counterparts, suggests tumor-driven epigenetic silencing of immune effector pathways. This is further corroborated by GO enrichment showing suppressed stress response and signal transduction pathways in PDAC tissues indicative of a microenvironment favoring immune evasion.

The gene expression differences between PDAC PBMCs and healthy PBMCs were not significant, but there were notable differences in gene expression between PDAC tissues and adjacent normal tissues. The differential gene expression analysis reveals that, although there are relatively small differences in gene expression between DAC PBMCs (Peripheral Blood Mononuclear Cells from patients with ductal adenocarcinoma of the pancreas) and healthy PBMCs, the results of gene enrichment analysis indicate that genes related to cytoplasmic translation, translation, protein

DOI: 10.54254/2753-8818/2025.AU24072

metabolic process, gene expression, and macromolecule biosynthetic process are activated. Indeed, PDAC does cause alterations in gene expression within PBMCs, but these changes are not significant. The gene expression profiles of PDAC (pancreatic ductal adenocarcinoma) tissues differ significantly from those of adjacent healthy tissues.

Spatial transcriptomics results reveal an even distribution of macrophages and tumor cells within the tissues. Notably, several genes, including NOP53, CFB, PPA1, CFTR, GATM, SERPINB1, and ANPEP, are highly expressed in these tissues, with NOP53 exhibiting the highest expression level. Specifically, NOP53 is abundantly expressed in PDAC tissues and functions as a tumor suppressor gene. Following DNA damage in humans, the interaction between NOP53 and RPL11 is disrupted, causing RPL11 to translocate to the nucleoplasm. This translocation subsequently inhibits MDM2 and activates p53, thereby suppressing cell division. Additionally, NOP53 expression impedes the PI3K-AKT signaling pathway, promoting endogenous apoptosis and inhibiting anabolic metabolism in cells. Thus, NOP53's abundant expression in PDAC tissues serves to suppress the division and proliferation of cancer cells.SDPR gene is also expressed at higher levels in PDAC tissues compared to adjacent healthy tissues, acting as another tumor suppressor gene. It participates in cellular signal transduction by blocking the TGF-β signaling pathway, which inhibits the production of Treg cells and subsequently suppresses the epithelial-mesenchymal transition (EMT) phenotype in breast cancer cells, although its direct role in PDAC may require further investigation. STC1 is widely expressed in macrophages within tumor tissues and can inhibit their phagocytosis of dead tumor cells, thereby suppressing their antigen-presenting capacity and inhibiting the activation of T and B cells. In gene differential expression analyses, elevated levels of S100A4 were observed in both PBMCs from PDAC patients and in PDAC tissues. S100A4 can inhibit the translocation of p53 protein from the cytoplasm to the nucleus, reducing nuclear p53 protein levels, and also inhibit the transcriptional activity of p53, thereby promoting PDAC progression. STC1 can upregulate S100A4 expression by promoting the phosphorylation of EGFR and ERK signals, exacerbating the malignancy of PDAC. The expression of SPP1 is upregulated in PDAC tissues. The CXCL9:SPP1 ratio plays a role in determining the polarity of tumor cells, and the upregulation of SPP1 expression may promote tumor growth, invasion, and metastasis. However, the expression product of SPP1 is also a cytokine that can upregulate the expression of interferon-γ (IFN-γ) and interleukin-12 (IL-12) while reducing the production of interleukin-10 (IL-10). IFN-γ and IL-12 are important antitumor immune factors that can activate immune cells and enhance their killing effect on tumor cells. In contrast, IL-10 is an anti-inflammatory factor that can inhibit the activity of immune cells, thereby favoring tumor growth and evading immune surveillance. Thus, SPP1 can both promote and inhibit the development of PDAC. The spatial co-localization of macrophages and tumor cells coupled with elevated NOP53 expression, positions NOP53 as a important node in PDAC biology. Beyond its canonical role in ribosomal biogenesis, NOP53's tumor-suppressive function via p53 activation and PI3K-AKT inhibition provides a dual therapeutic axis. Similarly, SPP1's paradoxical role:pro-metastatic via CXCL9:SPP1 imbalance yet immunostimulatory through IFN-γ/IL-123 induction.It emphasizes the need for context-specific targeting strategies.

In PDAC tissues, changes in gene expression lead to a reduction in the cytotoxicity of macrophages. By examining the differences in gene expression between tissue samples and healthy tissues, if the expression levels of genes such as NOP53, STC1, and SPP1 are elevated, it may indicate the presence of PDAC. This can be used for early diagnosis of cancer occurrence, facilitating subsequent treatment.

5. Conclusion

This study integrates single-cell and spatial transcriptomics to unravel the spatiotemporal dynamics of TAMs in PDAC. We demonstrate that PDAC-associated macrophages exhibit spatially expanded distributions and epigenetically silenced cytotoxic pathways, contrasting with their healthy

DOI: 10.54254/2753-8818/2025.AU24072

counterparts. Key molecular nodes, including NOP53 and SPP1, were identified as central players in PDAC progression and immune evasion. Spatial transcriptomic profiling further highlights ribosomal biogenesis and cytoplasmic translation as PDAC-enriched pathways, with elevated expression gradients of NOP53, CFB, and SPP1 serving as potential diagnostic biomarkers. These findings underscore the therapeutic potential of targeting macrophage-driven immunosuppression and metabolic reprogramming while emphasizing the need for context-specific strategies to address the roles of molecular hubs in PDAC biology.

References

[1] *Chouari, T. et al. Advances in Immunotherapeutics in Pancreatic Ductal Adenocarcinoma. Cancers 15, 4265 (2023).*
[2] *Ilic, M. & Ilic, I. Epidemiology of pancreatic cancer. World J. Gastroenterol. 22, 9694 (2016).*
[3] *Klein, A. P. Pancreatic cancer epidemiology: understanding the role of lifestyle and inherited risk factors. Nat. Rev. Gastroenterol. Hepatol. 18, 493–502 (2021).*
[4] *Ho, T. T. B. et al. Combination of gemcitabine and anti-PD-1 antibody enhances the anticancer effect of M1 macrophages and the Th1 response in a murine model of pancreatic cancer liver metastasis. J. Immunother. Cancer 8, e001367 (2020).*
[5] *Zhu, Y. et al. CSF1/CSF1R Blockade Reprograms Tumor-Infiltrating Macrophages and Improves Response to T-cell Checkpoint Immunotherapy in Pancreatic Cancer Models. Cancer Res. 74, 5057–5069 (2014).*
[6] *Locati, M., Curtale, G. & Mantovani, A. Diversity, Mechanisms, and Significance of Macrophage Plasticity. Annu. Rev. Pathol. Mech. Dis. 15, 123–147 (2020).*
[7] *Wynn, T. A., Chawla, A. & Pollard, J. W. Macrophage biology in development, homeostasis and disease. Nature 496, 445–455 (2013).*
[8] *Mantovani, A., Marchesi, F., Malesci, A., Laghi, L. & Allavena, P. Tumour-associated macrophages as treatment targets in oncology. Nat. Rev. Clin. Oncol. 14, 399–416 (2017).*
[9] *Wu, Y. et al. Macrophage cell membrane-based nanoparticles: a new promising biomimetic platform for targeted delivery and treatment. J. Nanobiotechnology 20, 542 (2022).*
[10] *Cai, H., Zhang, Y., Wang, J. & Gu, J. Defects in Macrophage Reprogramming in Cancer Therapy: The Negative Impact of PD-L1/PD-1. Front. Immunol. 12, 690869 (2021).*
[11] *Ruffell, B. & Coussens, L. M. Macrophages and Therapeutic Resistance in Cancer. Cancer Cell 27, 462–472 (2015).*
[12] *DeNardo, D. G. & Ruffell, B. Macrophages as regulators of tumour immunity and immunotherapy. Nat. Rev. Immunol. 19, 369–382 (2019).*
[13] *Ngambenjawong, C., Gustafson, H. H. & Pun, S. H. Progress in tumor-associated macrophage (TAM)-targeted therapeutics. Adv. Drug Deliv. Rev. 114, 206–221 (2017).*
[14] *Dai, E. et al. Autophagy-dependent ferroptosis drives tumor-associated macrophage polarization via release and uptake of oncogenic KRAS protein. Autophagy 16, 2069–2083 (2020).*
[15] *Mehla, K. & Singh, P. K. Metabolic Regulation of Macrophage Polarization in Cancer. Trends Cancer 5, 822–834 (2019).*
[16] *Fendl, B., Berghoff, A. S., Preusser, M. & Maier, B. Macrophage and monocyte subsets as new therapeutic targets in cancer immunotherapy. ESMO Open 8, 100776 (2023).*
[17] *Wei, C. et al. Crosstalk between cancer cells and tumor associated macrophages is required for mesenchymal circulating tumor cell-mediated colorectal cancer metastasis. Mol. Cancer 18, 64 (2019).*
[18] *Wu, K. et al. Redefining Tumor-Associated Macrophage Subpopulations and Functions in the Tumor Microenvironment. Front. Immunol. 11, 1731 (2020).*
[19] *Seyfried, T. N. & Huysentruyt, L. C. On the Origin of Cancer Metastasis. Crit. Rev. Oncog. 18, 43–73 (2013).*
[20] *Cao, L., Meng, X., Zhang, Z., Liu, Z. & He, Y. Macrophage heterogeneity and its interactions with stromal cells in tumour microenvironment. Cell Biosci. 14, 16 (2024).*
[21] *Zhang, X., Ji, L. & Li, M. O. Control of tumor-associated macrophage responses by nutrient acquisition and metabolism. Immunity 56, 14–31 (2023).*
[22] *Rao, L. et al. Activating Macrophage-Mediated Cancer Immunotherapy by Genetically Edited Nanoparticles. Adv. Mater. 32, 2004853 (2020).*
[23] *Gao, J., Liang, Y. & Wang, L. Shaping Polarization Of Tumor-Associated Macrophages In Cancer Immunotherapy. Front. Immunol. 13, 888713 (2022).*
[24] *Mills, C. D., Lenz, L. L. & Harris, R. A. A Breakthrough: Macrophage-Directed Cancer Immunotherapy. Cancer Res. 76, 513–516 (2016).*
[25] *Wang, H., Yung, M. M. H., Ngan, H. Y. S., Chan, K. K. L. & Chan, D. W. The Impact of the Tumor Microenvironment on Macrophage Polarization in Cancer Metastatic Progression. Int. J. Mol. Sci. 22, 6560 (2021).*

DOI: 10.54254/2753-8818/2025.AU24072

[26] Li, M. et al. Metabolism, metabolites, and macrophages in cancer. J. Hematol. Oncol.J Hematol Oncol 16, 80 (2023).

[27] Halbrook, C. J. et al. Macrophage-Released Pyrimidines Inhibit Gemcitabine Therapy in Pancreatic Cancer. Cell Metab. 29, 1390-1399.e6 (2019).

[28] Menjivar, R. E. et al. Arginase 1 is a key driver of immune suppression in pancreatic cancer. eLife 12, e80721 (2023).

[29] Kuen, J., Darowski, D., Kluge, T. & Majety, M. Pancreatic cancer cell/fibroblast co-culture induces M2 like macrophages that influence therapeutic response in a 3D model. PLOS ONE 12, e0182039 (2017).

[30] LaRue, M. M. et al. Metabolic reprogramming of tumor-associated macrophages by collagen turnover promotes fibrosis in pancreatic cancer. Proc. Natl. Acad. Sci. 119, e2119168119 (2022).

[31] Kemp, S. B. et al. Apolipoprotein E Promotes Immune Suppression in Pancreatic Cancer through NF-κB–Mediated Production of CXCL1. Cancer Res. 81, 4305–4318 (2021).

[32] Kemp, S. B. et al. Pancreatic cancer is marked by complement-high blood monocytes and tumor-associated macrophages. Life Sci. Alliance 4, e202000935 (2021).

[33] Padoan, A., Plebani, M. & Basso, D. Inflammation and Pancreatic Cancer: Focus on Metabolism, Cytokines, and Immunity. Int. J. Mol. Sci. 20, 676 (2019).

[34] Lee, B. Y. et al. Heterocellular OSM-OSMR signalling reprograms fibroblasts to promote pancreatic cancer growth and metastasis. Nat. Commun. 12, 7336 (2021).

[35] Lankadasari, M. B., Mukhopadhyay, P., Mohammed, S. & Harikumar, K. B. TAMing pancreatic cancer: combat with a double edged sword. Mol. Cancer 18, 48 (2019).

[36] Yang, Y. et al. M2 Macrophage-Derived Exosomes Promote Angiogenesis and Growth of Pancreatic Ductal Adenocarcinoma by Targeting E2F2. Mol. Ther. 29, 1226–1238 (2021).

[37] Gross, A. et al. Technologies for Single-Cell Isolation. Int. J. Mol. Sci. 16, 16897–16919 (2015).

[38] Nasir, I. et al. Tumor macrophage functional heterogeneity can inform the development of novel cancer therapies. Trends Immunol. 44, 971–985 (2023).

[39] Yang, K., Yang, T., Yu, J., Li, F. & Zhao, X. Integrated transcriptional analysis reveals macrophage heterogeneity and macrophage-tumor cell interactions in the progression of pancreatic ductal adenocarcinoma. BMC Cancer 23, 199 (2023).

[40] Marx, V. Method of the Year: spatially resolved transcriptomics. Nat. Methods 18, 9–14 (2021).

[41] Gerlinger, M. et al. Intratumor Heterogeneity and Branched Evolution Revealed by Multiregion Sequencing. N. Engl. J. Med. 366, 883–892 (2012).

[42] Multimodal Mapping of the Tumor and Peripheral Blood Immune Landscape in Human Pancreatic Cancer (https://www.ncbi.nlm.nih.gov/geo/query/acc.cgi?acc=GSE155698)

[43] Pancreatic Cancer with Xenium Human Multi-Tissue and Cancer Panel (https://www.10xgenomics.com/datasets/pancreatic-cancer-with-xenium-human-multi-tissue-and-cancer-panel-1-standard)